

Quantum Gates and Decoherence

Stefan Scheel¹, Jiannis Pachos², E.A. Hinds¹, and Peter L. Knight¹

¹ Quantum Optics and Laser Science, Blackett Laboratory, Imperial College
London, Prince Consort Road, London SW7 2BW, United Kingdom
s.scheel@imperial.ac.uk

² DAMTP, Centre for Mathematical Sciences, Wilberforce Road, Cambridge CB3
0WA, United Kingdom.

”God forbid that we should give out a dream of our own imagination
for a Pattern of the World.”

— Francis Bacon, Novum Organum

1 Introduction

In this article we will be concerned with some possible physical realizations of quantum gates that are useful for quantum information processing. After a brief introduction into the subject, in Sec. 2 we will focus on a particular way of using atoms in one-dimensional optical lattices as carriers of the quantum information. In Sec. 3 on the contrary, the information carriers will be photons that interact via effective nonlinearities which arises from mixing at passive linear optical elements and postselection through photodetection. These two seemingly different implementations have in common that their decoherence mechanism is described by a single theory, namely that of quantum electrodynamics in causal media which will be the subject of Sec. 4. Figure 1 should serve as an overview of the subject areas covered.

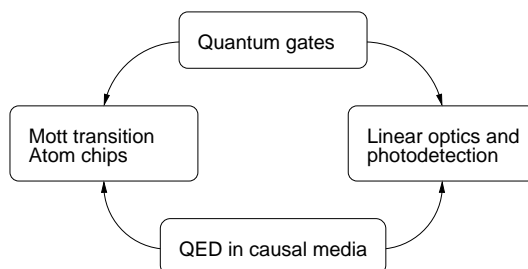


Fig. 1. Connections between the subject areas covered.

1.1 Why quantum information processing?

Apart from the academically driven curiosity to learn more about information in a quantum-mechanical setting, there is very urgent practical need to investigate information processing and computing from a quantum theory point of view. Over the last 30 years the number of transistors on an integrated circuit, i.e. the complexity of the computer made up from those chips, doubles roughly every 18 months. This empirical behaviour is famously known as Moore's first law (after the co-founder of Intel Corp., G. Moore). An extrapolation reveals that by the year 2017 a bit of information will need to be encoded in a single atom. Even if Moore's law breaks down before we eventually come to this point, at the current growth rate, by the year 2012 the dimensions of logical elements will be so small that quantum effects upon computation cannot be neglected any longer.³ Thus, technological progress necessitates the study of what implications quantum theory has on computation.

Another reason for looking deeper into quantum computing lies in the potential ability to simulate the temporal evolution of (possibly chaotic) quantum systems. The intrinsic and potentially massive parallelism of quantum computers that stems from linearity of quantum mechanics and the resulting superposition principle, would allow to investigate quantum Hamiltonian systems without the need for an exponential temporal overhead on a classical computer (see e.g. [1]).

1.2 Quantum gates vs. classical gates

"Information is physical."
— Rolf Landauer

The most important difference between a logical gate known from classical information processing and a quantum gate is its reversibility or conservation of information. In order to see what that means, let us consider for example the logical NAND gate whose action of logical 0's and 1's are given by the truth table 1. Equivalently, we can describe it by the action of $\overline{X_1} \wedge \overline{X_2}$ on two Boolean variables X_1 and X_2 . This gate is generic for classical gates in that it has two (or more) inputs and only a single output. In quantum mechanics, we are allowed to form linear combinations or superpositions of the logical basis states, i.e. $c_0|00\rangle + c_1|01\rangle + c_2|10\rangle + c_3|11\rangle$. The formal application of the classical NAND on this quantum superposition would result in a state $\propto c_3|0\rangle + (c_0 + c_1 + c_2)|1\rangle$. The resulting state contains far less information than the original state. Whereas before the gate operation all the weight coefficients c_i gave us information about the quantum state, after the action

³The most recent Intel Pentium 4 processor already contains features of the size of 90nm, i.e. 900Å. The lithography used to generate such structures therefore uses XUV light!

Table 1. Truth table of the logical NAND gate

inputs	output
00	1
01	1
10	1
11	0

of the classical NAND only the *sum* $c_0 + c_1 + c_2$ plays a rôle in determining the weight of the logical $|1\rangle$. All the information about the mutual *differences* are lost during the operation. However, this state is obviously not properly normalized anymore. The formal action of a classical gate is therefore actually an ill-posed operation in quantum mechanics. In fact, there is no way of making sense of classical logical operations acting on quantum superpositions.

In quantum information processing, all operations have to be unitary. This means on one hand that the number of output degrees of freedom must equal the number of input degrees of freedom, and on the other hand it means that no information is lost about an initial superposition. In general, we could allow even more general operations such as completely positive maps of which the unitary operations are a subset. However, not even using the correct number of inputs and outputs together with no loss of information is sufficient to define a quantum operation. For example, let us consider an operation in which a given quantum state $c_0|0\rangle + c_1|1\rangle$ is transformed into its orthogonal complement, hence into the state $-c_1^*|0\rangle + c_0^*|1\rangle$. This operation could be thought of as being the analogue of the classical NOT operation which is defined as $X \mapsto \bar{X} : \bar{X} \wedge X = 0$. However, it turns out that the quantum-NOT operation is not a completely positive map and therefore cannot be implemented by any quantum circuit. In fact, the map describing this transformation is anti-unitary [2] with determinant -1 .⁴

Universal set of quantum gates

Now we have shown that there is no strict connection between classical logical gates and quantum mechanics, we will next briefly discuss which operations are compatible with quantum mechanics. Let us first look into operations acting on a single logical qubit state $c_0|0\rangle + c_1|1\rangle$. The dynamical group associated with this state is the unitary group $SU(2)$ whose action can be given in terms of its generators, the Pauli spin operators $\hat{\sigma}_i$ ($i = x, y, z$), as $\hat{U} = e^{i\boldsymbol{\alpha}\cdot\hat{\boldsymbol{\sigma}}}$. Here, $\boldsymbol{\alpha}$ denotes the direction of the rotation axis and the associated rotation angle. By decomposing \hat{U} into exponential factors, one can derive the so-called Euler decomposition $\hat{U} = e^{ia_1\hat{\sigma}_z} e^{ia_2\hat{\sigma}_y} e^{ia_3\hat{\sigma}_z}$ which

⁴In this context, the notion of universal gate has been invented. A universal NOT-gate would be the one that, when averaging over all input state, comes closest to the NOT-operation.

just describes a sequence of elementary rotations. The Pauli operators have the following representation in the single-qubit basis:

$$\hat{\sigma}_x = |0\rangle\langle 1| + |1\rangle\langle 0|, \quad (1)$$

$$\hat{\sigma}_y = i(|0\rangle\langle 1| - |1\rangle\langle 0|), \quad (2)$$

$$\hat{\sigma}_z = |0\rangle\langle 0| - |1\rangle\langle 1|. \quad (3)$$

An equivalent set of operators would be $\hat{\sigma}_\pm = \hat{\sigma}_x \pm i\hat{\sigma}_y$ and $\hat{\sigma}_z$ which results in an operator decomposition of the form $\hat{U} = e^{ib_1(1+\hat{\sigma}_z)} e^{ib_2\hat{\sigma}_+} i e^{b_3\hat{\sigma}_-} i e^{b_4(1-\hat{\sigma}_z)}$. This result will be used later in Sec. 3 to describe beam splitters.

By definition, the Pauli operators are enough to represent all other single-qubit operations. An important example is the Hadamard gate \hat{H} (not to be confused with the Hamiltonian),

$$\hat{H} = \frac{1}{\sqrt{2}} \left[(|0\rangle + |1\rangle)\langle 0| + (|0\rangle - |1\rangle)\langle 1| \right], \quad (4)$$

which transform logical states into coherent superpositions. From the definition of the Pauli operators it is obvious that the Hadamard gate can be written as $\hat{H} = (\hat{\sigma}_x + \hat{\sigma}_z)/\sqrt{2}$.

As for two-qubit gates, the structure of the unitary operator associated with the dynamical symmetry is not so obvious. We will therefore restrict our attention to some particularly useful gates. One of the most important nontrivial two-qubit gates is the controlled-phase gate \hat{C}_φ whose truth table is given in Table 2. The controlled-phase gate (or its special case the

Table 2. Truth table of the controlled-phase gate

input	output
$ 00\rangle$	$ 00\rangle$
$ 01\rangle$	$ 01\rangle$
$ 10\rangle$	$ 10\rangle$
$ 11\rangle$	$e^{i\varphi} 11\rangle$

controlled- $\hat{\sigma}_z$ gate with $\varphi = \pi$), together with the set of Pauli operators, forms a universal set of quantum gates [3] by which we mean that all possible quantum networks can be build up from them. Therefore, if one is able to build these four gates, one can generate arbitrary quantum operations by concatenating them (Fig. 2).

For example, another nontrivial two-qubit gate is the controlled-NOT (or CNOT) under whose action the logical states $|10\rangle$ and $|11\rangle$ are exchanged and the other left untouched.⁵ This operator can be realized by the combination

⁵The associated operator can be written as $|0\rangle\langle 0| \otimes \hat{I} + |1\rangle\langle 1| \otimes \hat{\sigma}_z$.

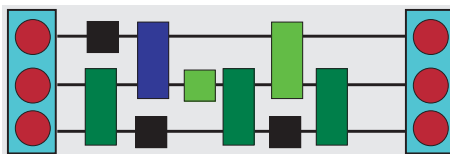


Fig. 2. A quantum network can be build from a universal set of quantum gates. Here we sketch a three bit register which is manipulated by a sequence of one and two qubit gates to realize a chosen unitary transformation which effects the relevant algorithm.

$\hat{H}_1 \hat{C}_\pi \hat{H}_1$, i.e. by two Hadamard gates acting on mode 1 and a controlled- $\hat{\sigma}_z$ gate. Other two-qubit gates of importance are the swap in which the qubits are simply exchanged and the square root of swap which serves as an entangling gate.

2 Atomic realisation — atom chips and the Mott transition in optical lattices

There are many possible realizations of quantum bits: laser-cooled trapped ions, cold trapped neutral atoms, atoms in high-Q single-mode cavities as well as condensed matter candidates such as quantum dots or Josephson junctions. For any one of these to be viable, the effects of the environment (dissipation and temperature) must be minimized, if not entirely eradicated. This simply means we need to use cold state initialization.

In this section, we will describe a possible way of implementing quantum computation with cold atom technology. This includes the application of optical lattices in a sufficiently cold cloud of atoms showing Bose-Einstein condensation (BEC). The lasers which generate the periodic spatially varying trapping potential through the AC Stark effect create an optical lattice strong enough to induce a quantum phase transition from the superfluid phase that characterises the BEC to the Mott insulator phase, characterised by a regular structure of one atom per lattice site that can serve as a quantum register. A universal set of quantum gates can then be realised by manipulations of the lattice potential with additional laser fields.

2.1 Bose–Einstein condensates and the Mott transition

In recent years it has been realized that Bose–Einstein condensates (BECs for short) can undergo a phase transition if loaded into a three-dimensional periodic potential which for example can be realized by standing-wave optical fields [4]. That is, one starts off with a BEC in its superfluid phase in which the relative phases (or rather correlations) between the atoms are well-defined such that the whole ensemble of atoms can be described by a single



Fig. 3. Counter-propagating laser beams induce a periodic spatially varying trapping potential through the AC Stark shift.

macroscopic wave function (in first approximation). By loading this condensate into the optical lattice (see Fig. 3) the number of atoms per lattice site is undetermined and can vary widely. The ground-state wave function for N atoms in a lattice with M sites is therefore

$$|\Psi_S\rangle \propto \left(\sum_{i=1}^M \hat{a}_i^\dagger \right)^N |0\rangle \quad (5)$$

where the \hat{a}_i^\dagger denote creation operators of an atom at the lattice site i . However, when increasing the strength of the potential by increasing the power of the laser beams that create the standing-wave potential, eventually there will be a phase-transition to a state of the condensate in which each lattice site is occupied by a fixed and well-defined number of atoms (ideally we would like to have exactly one atom per site). In this so-called Mott-insulator phase the relative phases (or correlations) between neighboring lattice sites are undetermined. The ground-state wave function here looks essentially like

$$|\Psi_M\rangle \propto \prod_{i=1}^M (\hat{a}_i^\dagger)^n |0\rangle \quad (6)$$

where n is the number of atoms per lattice site. Experimental evidence of this phase-transition has been obtained in the beautiful experiments described in [5, 6]. Although a Bose–Einstein condensate really exists only in three dimensions (since only there we find a phase transition from a thermal cloud to a condensate), there are analogous systems such as the quasi-condensate [7] and the Tonks–Girardeau gas [8] in one dimension that have similar properties.

The effective interaction Hamiltonian that can be derived from the Gross–Pitaevskii equation under the assumption that the atoms have localized single-particle wave functions can be written as

$$\hat{H} = \frac{U}{2} \sum_i \hat{n}_i(\hat{n}_i - 1) - J \sum_i (\hat{a}_i^\dagger \hat{a}_{i+1} + \hat{a}_{i+1}^\dagger \hat{a}_i). \quad (7)$$

This Hamiltonian is also known in the literature as the Bose–Hubbard Hamiltonian. The first term with coupling strength U is the collisional energy of atoms occupying the same lattice site. Obviously, if there is zero or just

one atom per site, this term vanishes identically. The second term is the so-called hopping term which essentially is given by the overlap of the localized wavefunctions at neighboring sites and describes tunneling between adjacent lattice sites with tunneling strength J . If, for example, the optical lattice is formed by the standing wave of a one-dimensional cavity mode having width L , the trapping potential is given by

$$V(x) = -V_0 \sin^2 kx \exp\left(-\frac{2r^2}{L^2}\right) \quad (8)$$

where r denotes the transverse distance from the lattice axis and k the wave number of the standing wave. With this potential, the collisional strength can be approximated by

$$U \approx \frac{4a_s V_0^{3/4} E_R^{1/4}}{\sqrt{\lambda L}} \quad (9)$$

where a_s is the scattering length of the atomic collisions and E_R the atomic recoil energy. An analogous derivation shows that the tunneling rate can be expressed as

$$J \approx \frac{E_R}{2} \exp\left(-\frac{\pi^2}{4} \sqrt{\frac{V_0}{E_R}}\right) \left[\sqrt{\frac{V_0}{E_R}} + \left(\sqrt{\frac{V_0}{E_R}}\right)^3 \right]. \quad (10)$$

It is now apparent that by changing the potential depth V_0 one can tune the system of atoms into either of the two (superfluid or Mott-insulator) phases as seen in Fig. 4. For example, if V_0 is relatively small compared

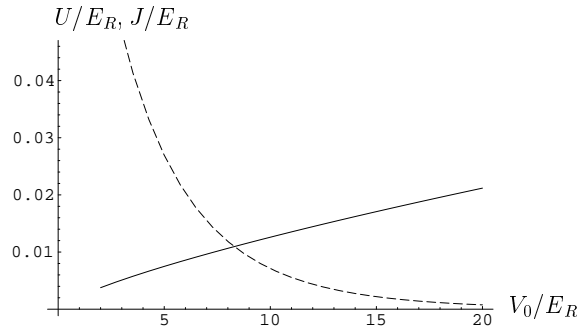


Fig. 4. The values of U/E_R (solid line) and J/E_R (dashed line) are plotted against V_0/E_R for typical values of the relevant length scales appearing in Eq. (9) ($a_s = 5.6\text{nm}$ for ^{87}Rb , $L = \lambda = 10\mu\text{m}$).

to the recoil energy E_R , the tunneling rate J will be large and the atoms will be delocalized and form a superfluid. Increasing V_0 means exponentially

decreasing the tunneling rate and the atoms will become stuck in their respective potential wells and form the Mott-insulator phase. In Fig. 5 we show

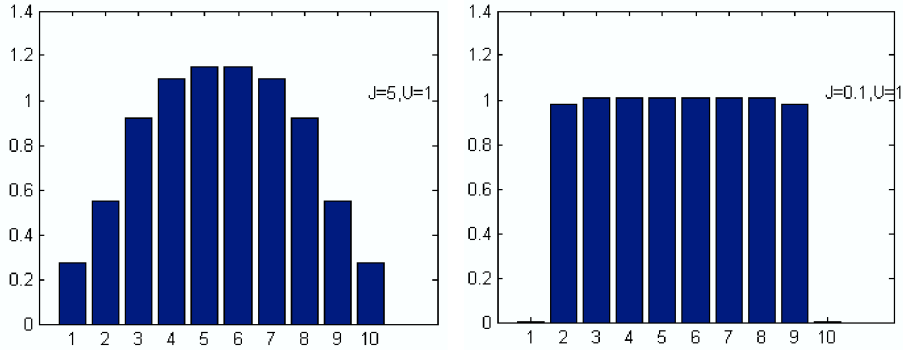


Fig. 5. Distribution of 8 atoms among 10 lattice sites in the limits $U/J \ll 1$ (left figure) and $U/J \gg 1$ (right figure).

an example calculation for the population distribution in a one-dimensional lattice with 10 sites occupied by 8 atoms. The figure on the left depicts a situation in which the collisional energy U is small compared to the tunneling rate J ($U/J \ll 1$) and hence a superfluid phase exists, witnessed by a Gaussian-like distribution. On the other hand, the figure on the right shows the one-by-one distribution of atoms for $U/J \gg 1$ which closely resembles a Fock state at each site. In fact, the critical value for obtaining the phase-transition is $U/J \approx 11.6$ [9]. Note that the calculation of the ground-state wave function can only be done numerically which amounts to computing the eigenvector corresponding to the smallest eigenvalue of a sparse matrix of dimension $\binom{A+W-1}{A}$, where A is the number of atoms in W lattice sites.

2.2 Quantum computation with a 1D optical lattice

In order to use the Mott-insulator phase for building a quantum register, it is advantageous to use atoms with two degenerate ground states $|g_a\rangle$ and $|g_b\rangle$ which are coupled to each other with a Raman transition via an excited state [10]. In order to trap both ‘species’ of atoms simultaneously, an optical lattice formed of two counterpropagating laser beams with parallel linear polarization vectors is needed. The result of this configuration is that the atoms are trapped in two overlapping optical lattices with polarizations σ_+ and σ_- each of which can trap one of the two atomic ground states.

If we denote the creation operators of atoms in the states $|g_a\rangle$ and $|g_b\rangle$ by \hat{a}^\dagger and \hat{b}^\dagger , respectively, we can write the interaction Hamiltonian (7) as

$$\hat{H} = \sum_i \left[\frac{U_{aa}}{2} \hat{n}_i^a (\hat{n}_i^a - 1) + U_{ab} \hat{n}_i^a \hat{n}_i^b + \frac{U_{bb}}{2} \hat{n}_i^b (\hat{n}_i^b - 1) \right]$$

$$- \sum_i \left(J_i^a \hat{a}_i^\dagger \hat{a}_{i+1} + J_i^b \hat{b}_i^\dagger \hat{b}_{i+1} + J_i^R \hat{a}_i^\dagger \hat{b}_i + \text{h.c.} \right). \quad (11)$$

Here we encounter several couplings amongst atoms of the same species (collisional couplings U_{aa} , U_{bb} and tunneling rates J^a , J^b) as well as coupling of atoms of different species (collisional coupling U_{ab} and effective Raman coupling J^R).

We assume that initially all atoms are in the ground state $|g_a\rangle$. This is the state which from now on will be denoted by $|0\rangle$ whereas the second ground state $|g_b\rangle$ will serve as the logical $|1\rangle$.

Single-qubit rotations

From the above definition of the logical states it is clear that single-qubit rotations can be performed by a Raman process. For example, starting at $|0\rangle$ and performing half a Raman cycle leaves us with an atom in state $|1\rangle$, whereas shorter interactions produce superposition states between $|0\rangle$ and $|1\rangle$. If one starts from an arbitrary superposition, the application of a full Raman cycle generates an effective $\hat{\sigma}_x$ -rotation. In addition, a simple Rabi cycle of 2π applied to the ground state $|g_b\rangle$ is equivalent to changing the phase of the logical $|1\rangle$ by π and thus represents a σ_z operation.

Two-qubit gates — controlled-phase gate and square root of the swap operator

In order to realize two-qubit operations, we need to couple two atoms in neighboring lattice sites to each other in a controlled way. Let us assume that the lattice is sufficiently deep such that without external changes tunneling between lattice sites is prohibited, hence J^a and J^b can be initially neglected. A tunneling coupling between neighboring sites can be switched on by applying an additional standing wave perpendicular to the lattice with a waist that should not exceed the size of two lattice sites (see Fig. 6). Depending on the

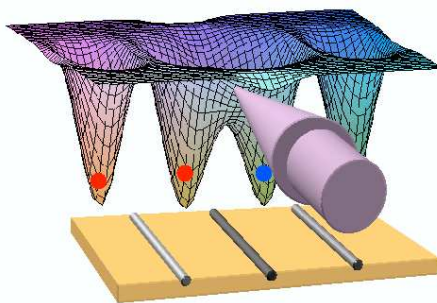


Fig. 6. The tunneling interaction between neighboring lattice sites can be switched on by lowering the potential barrier between the sites.

circular polarization (σ_+ or σ_-) of the additional laser beam the tunneling strength for both atomic species can be tuned independently.

For the two-qubit operations to work, the tunneling coupling must always be much smaller than the collisional coupling, even when the potential barrier has been lowered. Hence, we require $U \gg J$ for all times during the interaction process. This amounts to the fact that the system stays in the eigenspace of the collisional terms U_{aa} and U_{bb} , hence in a number state. This eigenspace is in fact degenerate with respect to the occupation numbers $n_{a,b} = 0$ and $n_{a,b} = 1$ since the collisional energy is obviously zero in both cases. There is an energy gap from this degenerate subspace to the state with two atoms of the same species per lattice site which means that those states can be adiabatically eliminated from the evolution. If, in addition, there is a large inter-species collisional coupling U_{ab} , then the same energy gap persists even for states in which two atoms of different species occupy one lattice site. Thus, every state with more than one atom per lattice site, regardless of their species, can be adiabatically eliminated thereby leaving us with a degenerate eigenspace spanned by the logical states $|0\rangle = |n_a = 1, n_b = 0\rangle$ and $|1\rangle = |n_a = 0, n_b = 1\rangle$. This constitutes our well-defined computational space.

In what follows, we will use the notation introduced in [10] by denoting the state of the atomic population in two lattice sites by $|n_a^1, n_b^1; n_a^2, n_b^2\rangle$. Then, for example, a state of two atoms in their respective ground states $|g_b\rangle$ is given in this notation by $|01; 01\rangle$ and represents the logical two-qubit state $|11\rangle$. Suppose now we were to lower the potential barrier between two neighboring sites only for the atom in ground state $|g_b\rangle$ which can be done by choosing an appropriate polarization of the incident laser beam. Then, according to the Hamiltonian (11), this state can couple to only two other states, $|02; 00\rangle$ and $|00; 02\rangle$, with two atoms simultaneously at one lattice site. The Hamiltonian (11) can be written in the basis $\{|01; 01\rangle, |02; 00\rangle, |00; 02\rangle\}$ as

$$H_{bb} = \begin{pmatrix} 0 & -J^b & -J^b \\ -J^b & U_{bb} & 0 \\ -J^b & 0 & U_{bb} \end{pmatrix}. \quad (12)$$

This Hamiltonian effectively corresponds to a V -system with ground state $|01; 01\rangle$ and excited states $|02; 00\rangle, |00; 02\rangle$ coupled by an effective Rabi frequency $-J^b/2$ and detuned by U_{bb} (see left figure in Fig. 7). Assuming that the detuning is large, the system remains in the ground state and acquires a phase $-2 \int dt (J^b)^2/U_{bb}$. However, in the same manner the logical states $|01\rangle = |1, 0; 0, 1\rangle$ and $|10\rangle = |0, 1; 1, 0\rangle$ acquire phases. This is due to their interaction with the states $|1, 1; 0, 0\rangle$ and $|0, 0; 1, 1\rangle$, respectively. For example, in the basis $\{|1, 0; 0, 1\rangle, |1, 1; 0, 0\rangle\}$ the Hamiltonian (11) simply reads

$$H_{ab} = \begin{pmatrix} 0 & -J^b \\ -J^b & U_{ab} \end{pmatrix} \quad (13)$$

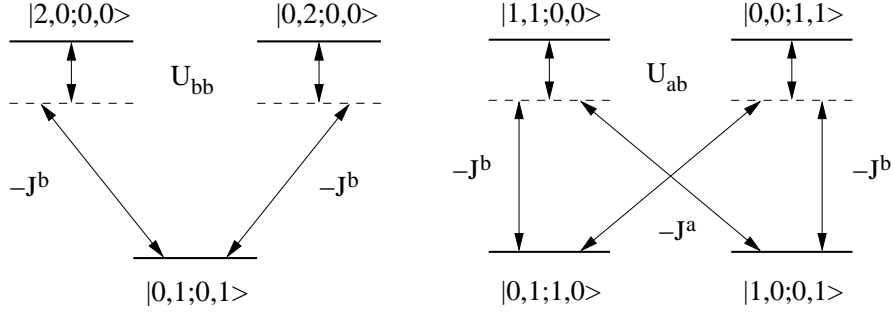


Fig. 7. Effective 3-level system coupling the state $|0, 1; 0, 1\rangle$ to its excited states (left figure), and effective 4-level system coupling $|0, 1; 1, 0\rangle$ and $|1, 0; 0, 1\rangle$ to their respective excited states (right figure).

which leads to a phase shift of $\int dt (J^b)^2/U_{ab}$. The latter can be compensated for by applying a single-qubit rotation on the state $|1\rangle$ on both lattice sites. The overall effect is to introduce a phase shift

$$\varphi = 2 \int_0^T dt \left(\frac{(J^b)^2}{U_{ab}} - \frac{(J^b)^2}{U_{bb}} \right) \quad (14)$$

to the logical state $|11\rangle$ while keeping all other logical basis states unchanged. This is the controlled-phase gate which, together with the single-qubit rotations, constitutes a universal set of operations for quantum computing.

Similarly, we can choose to act upon the logical states $|01\rangle$ and $|10\rangle$ which contain one atom of each species in neighboring lattice sites. In the adiabatic approximation, the Hamiltonian connecting these two states is (in the basis $\{|1, 1; 0, 0\rangle, |1, 0; 0, 1\rangle, |0, 1; 1, 0\rangle, |0, 0; 1, 1\rangle\}$, see right figure in Fig. 7)

$$H_{ab} = \begin{pmatrix} U_{ab} & -J^a & -J^b & 0 \\ -J^a & 0 & 0 & -J^b \\ -J^b & 0 & 0 & -J^a \\ 0 & -J^b & -J^a & U_{ab} \end{pmatrix} \quad (15)$$

with the solution that the following transformation on the logical states $|01\rangle$ and $|10\rangle$ is achieved:

$$|01\rangle \mapsto e^{-i\varphi} [\cos I|01\rangle - i \sin I|10\rangle] \quad (16)$$

$$|10\rangle \mapsto e^{-i\varphi} [-i \sin I|01\rangle + \cos I|10\rangle] \quad (17)$$

with

$$\varphi = \int_0^T dt \frac{(J^a)^2 + (J^b)^2}{U_{ab}}, \quad I = 2 \int_0^T dt \frac{J^a J^b}{U_{ab}}. \quad (18)$$

The effective Hamiltonian is therefore just

$$H_{\text{eff}} = -I(|10\rangle\langle 01| + |01\rangle\langle 10|), \quad (19)$$

which, for $I = \pi/4$ is also known also the square root of the swap operator. Additionally, the logical states $|00\rangle$ and $|11\rangle$ acquire phases $-2 \int dt (J^a)^2/U_{aa}$ and $-2 \int dt (J^b)^2/U_{bb}$, respectively, as discussed before. Thus, the two qubits pick up only an *overall* phase if one chooses $(J^a)^2/U_{aa} + (J^b)^2/U_{bb} = [(J^a)^2 + (J^b)^2]/U_{ab}$. This overall phase can later be reversed by applying appropriate single-qubit rotations on both lattices sites.

These examples show that it should be straightforward in principle to implement different types of single- and two-qubit operations with very few laser pulses (typically just one). The drawback is that for all above considerations the adiabaticity condition must be fulfilled. Thus, the couplings J^a and J^b are assumed to be small compared to the collisional couplings U_{aa} , U_{bb} , and U_{ab} which results in unwanted long gate evolution times. For example, in Ref. [10] it has been estimated that, for currently measured collisional couplings of $\mathcal{O}(1\text{kHz})$ [11], the gate operation time for nontrivial gates such as the above-described controlled-phase gate with an error rate less than 10^{-3} is roughly 100ms. This time scale is far too long to render quantum computation useful with this scheme. A way to circumvent this problem and to drastically reduce gate operation times is to relax the adiabaticity condition and to note that even without adiabatic evolution there are certain instances in which the atomic population returns completely to the logical space in which we have started. The drawback here is that laser amplitudes and pulse durations have to be stabilized much more precisely than in the adiabatic regime. Despite that, it seems that there is much potential in this and other proposals for quantum computing on an optical lattice.

Moreover, this time scale is already of the order of the currently possible trapping lifetime of atoms in recent experiments (see Sec. 4 for a detailed discussion about trapping losses). Hence, only a few gate operations can be performed before the atoms are lost from the optical lattice.

2.3 Experimental realization with atom chips

A particularly interesting way of implementing the above ideas of atomic registers is by using atom chips (for reviews on this exciting subject, see for example [12, 13]). The basic idea here is to trap cold atoms in one of their low-field seeking hyperfine ground states in the combined magnetic fields of a current-carrying wire and a constant transverse bias (see Fig. 8). The radial magnetic field of the wire is superimposed on a constant homogeneous field from the side thereby creating a line of zero magnetic field parallel to the wire. The atoms are thus trapped in a tubular region whose distance from the wire can be tuned by adjusting the relative strengths of the two overlapping magnetic fields. However, as depicted in the inset of Fig. 8, the atoms can flip

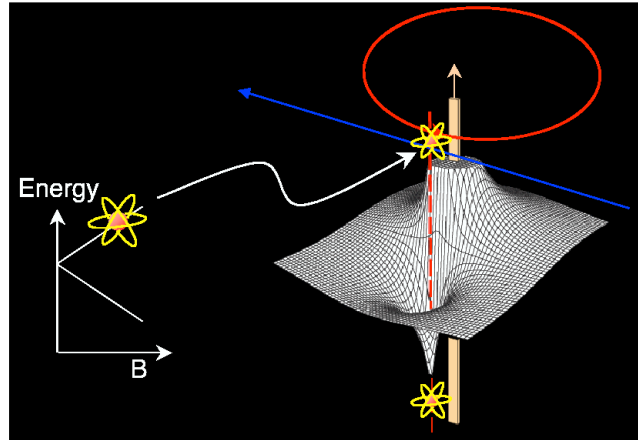


Fig. 8. Principle of the magnetic guide for atoms (see text for details).

their magnetic sublevels once they reach the region of zero magnetic field, hence yet another bias field has to be applied, this time parallel to the wire, to prevent the atoms from doing that.

Once the atoms are trapped and evaporatively cooled to form a Bose–Einstein condensate, the atom cloud has typically a length of $100\mu\text{m}$ and a diameter of $2\mu\text{m}$, hence it forms a long and thin cigar-shaped object which can be treated as quasi-1D. The idea is now to confine the cloud between two highly reflecting mirrors that form a microcavity in the standing wave of which the atoms experience the periodic light potential we were envisaging earlier (Fig.9). The idea is then to move a string of atoms [14] in a condensate

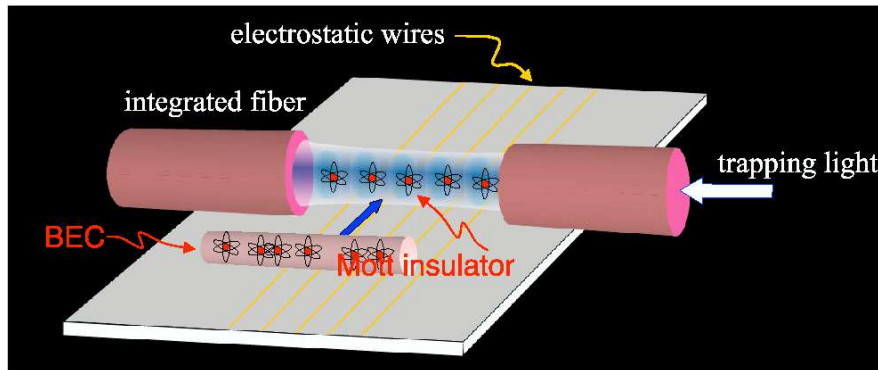


Fig. 9. Proposed scheme for combining atom chips with optical cavities for generating one-dimensional optical lattices.

state into the cavity region to perform the transition to the Mott-insulator. The current experimental status is that experiments have been performed in which a cloud of trapped atoms (not a BEC yet) has been moved in a ‘conveyor-belt’ fashion across the surface of a miniaturized atom chip. The next step will be to integrate two adjacent optical fibres with polished ends onto the atom chip to create the standing-wave potential.

An obvious performance limitation is given by the time the atoms actually spend in their respective trapped states above the wire. Several noise sources, both technical and fundamental, can cause spin flips from a trapped to an anti-trapped magnetic sublevel that will prevent the atoms from staying indefinitely above the wire surface. The influence of the predominant noise source — magnetic fluctuations caused by absorption in the current-carrying wire — will be investigated in more detail in Sec. 4.

3 Photonic realisation — passive linear optics and projective measurements

In a rather different setting compared to Sec. 2 we can consider photons as the carriers of quantum information. Photons constitute an alternative to atoms — being qubits at rest — as they are massless particles and therefore move at the speed of light which earned them the name ‘flying’ qubits. They will eventually be part of larger networks and are considered to be vital in transporting quantum information over longer distances. Moreover, it is believed that photons could even be used to perform quantum operations themselves. It is therefore vital to know what kind of operations can be done with photons and how they are implemented.

3.1 Qubit encoding and single-qubit operations

First of all, it is necessary to define which photonic degrees of freedom we would like to choose to encode our qubits in. One possibility would be to encode the information in the polarization state (horizontal or vertical) [15, 16], another one the superposition states of one photonic excitation in two modes [17]. Another, seemingly complementary encoding would use the photon number or Fock states of a photon. All the mentioned possibilities have their advantages and disadvantages. For example, single-qubit rotations are trivially implemented in the polarization basis because they are just performed by $\lambda/4$ - or $\lambda/2$ -plates. However, two-qubit operations such as the controlled-phase gate are impossible to implement in this way using wave plates.

In what follows we will look at an alternative encoding in which the qubits are defined by photon numbers. That is, the logical 0 will be the vacuum state of the electromagnetic field, and the logical 1 will be a single-photon Fock state. Then, let us consider a simple example of a two-qubit gate, the

controlled-phase gate defined by the truth table 2. That is, only the basis state containing one photon in each mode will pick up a phase φ , all other basis states are left unchanged.

Here we immediately encounter a problem in that, in order to realize this quantum gate, two single photons have to interact with each other sufficiently strongly to produce the desired phase shift. In fact, nature is not so kind as to allow us to do this easily. Consider for a moment standard quantum electrodynamics. The lowest-order Feynman diagram that contains a photon-photon interaction is depicted in Fig. 10. The interaction strength is of fourth order in the fine structure constant $\alpha \approx 1/137$ and therefore negligible.

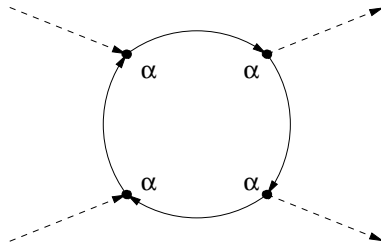


Fig. 10. Lowest-order Feynman diagram leading to a photon-photon interaction.

A seemingly promising alternative is provided by nonlinear materials exhibiting a $\chi^{(3)}$ or Kerr nonlinearity. The constituents of those materials respond nonlinearly to an external electromagnetic field, and after tracing out the matter degrees of freedom leaves behind an effective nonlinear interaction between photons. However, these natural nonlinearities are still too small to be of any use since only phase shifts of the order of 10^{-8} can be achieved.

3.2 Measurement-induced nonlinearities

A possible way out of this dilemma can be found in the use of so-called measurement-induced nonlinearities. The idea behind it is perfectly simple. Suppose we wanted to act on a pure single-mode state $|\psi\rangle$ with a nonlinear operator. In order to see this, we mix our signal state with another pure single-photon state at a beam splitter and perform a suitable projection measurement at one output port of the beam splitter. The result will be a *conditional* nonlinear operator acting on the signal mode. For example, let us consider the situation depicted in Fig. 11 in which a single-photon Fock state acts as our auxiliary (or ancilla) state. It is well-known that a beam splitter acts as an $SU(2)$ group element on the photonic amplitude operators [18]. Hence, the operator associated with the action of the beam splitter can be written in the two-mode representation of the Pauli operators (see Sec. 1) as [19]

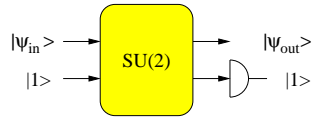


Fig. 11. Single beam splitter acting conditionally as a nonlinear operator.

$$\hat{U}_{12} = T^{\hat{n}_1} e^{-R^* \hat{a}_2^\dagger \hat{a}_1} e^{R \hat{a}_1^\dagger \hat{a}_2} T^{-\hat{n}_2} \quad (20)$$

where 1, 2 label the modes impinging on the beam splitter. Consider now the situation in which the auxiliary mode is prepared in a single-mode Fock state and a single photon is detected in the same output port. Then the resulting *conditional* operator acting on the signal mode reads

$$\hat{Y}_1 = \langle 1_2 | \hat{U}_{12} | 1_2 \rangle = T^{\hat{n}_1 - 1} [|T|^2 - \hat{n}_1 |R|^2]. \quad (21)$$

It is clear from the expression (21) that this operator represents a nonlinear evolution since it is inherently quartic in the photonic amplitude operators $\hat{a}_1^{(\dagger)}$. This is an *effective* nonlinearity since the overall evolution, counting the contributions from all possible measurement outcomes, is still perfectly *linear*. One observes furthermore that the operator \hat{Y}_1 is independent of the signal state, in fact, the nonlinearity is created by the measurement process only. Therefore, following the notation commonly used in quantum optics, this represents quantum-gate engineering — as opposed to quantum-state engineering — or, in other words, quantum-state engineering of arbitrary states. Note also that, on the other hand, in general the success probability $p = \|\hat{Y}_1 |\psi\rangle\|$ does depend on the chosen signal state $|\psi\rangle$. However, if the beam splitter parameters are chosen such that $\hat{Y}_1^\dagger \hat{Y}_1 |\psi\rangle \propto |\psi\rangle$, i.e. the conditional operator is proportional to a unitary operator (hence a quantum gate), then the success probability is state-independent as well. This important fact will be used later on to actually construct quantum gates with maximal success probability.

In order to go one step further in the development of conditional quantum gates for photons, we have to look at larger beam splitter networks consuming more than just one auxiliary or ancilla state. To do so, we note that every $U(N)$ transformation of N photonic amplitude operators can always be realized by a triangular-shaped network of at most $N(N-1)/2$ beam splitters and some phase shifters [20]. Hence, we need to generalize our arguments to whole networks of beam splitters. There seem to be essentially two ways of analyzing $U(N)$ networks. One is to look at the unitary operator $\hat{U}_{12\dots N}$ acting on N modes in terms of its Euler decomposition analogous to Eq. (20). Although this is not completely impossible, it is very tedious indeed. Moreover, the Euler decomposition has only been calculated for $N = 3, 4$ [21]. An alternative way has been developed in [22] and uses well-known techniques from bosonic operator algebras.

For this purpose, we write the input state — still assumed to be a single-mode state, the theory is analogous for multi-mode states — in a functional form as

$$|\psi\rangle = \hat{f}(\hat{a}_1^\dagger)|0\rangle = \sum_m \frac{c_m}{\sqrt{m!}} (\hat{a}_1^\dagger)^m |0\rangle, \quad (22)$$

where the c_m are constrained in such a way that $\sum_m |c_m|^2 = 1$. Analogously, we write the auxiliary state $|A\rangle$ and the state $|P\rangle$, respectively, in product form as

$$|A\rangle = \prod_{i=2}^N \frac{(\hat{a}_i^\dagger)^{m_i}}{\sqrt{m_i!}} |0\rangle^{\otimes N-1}, \quad |P\rangle = \prod_{j=2}^N \frac{(\hat{a}_j^\dagger)^{n_j}}{\sqrt{n_j!}} |0\rangle^{\otimes N-1}. \quad (23)$$

Here m_i is a non-negative integer that represents the number of photons initially in mode i , and n_j is the number of photons in the projected mode j . The beam splitter network is represented by a unitary $N \times N$ -matrix \mathbf{A} , under the action of which the amplitude operators transform as

$$\hat{\mathbf{a}} \mapsto \mathbf{A}^+ \hat{\mathbf{a}}, \quad \hat{\mathbf{a}}^\dagger \mapsto \mathbf{A}^T \hat{\mathbf{a}}^\dagger. \quad (24)$$

Combining all these definitions we derive the (un-normalised) output state after mixing at the beam splitter network and projecting onto $|P\rangle$ as

$$\begin{aligned} |\psi'\rangle &\propto \langle P | \hat{U}_{12\dots N} | A \rangle \otimes |\psi\rangle \\ &= {}^{N-1}\langle 0 | \prod_{i,j=2}^N \frac{(\hat{a}_j)^{n_j}}{\sqrt{m_i! n_j!}} \left(\sum_{k=1}^N \Lambda_{ki} \hat{a}_k^\dagger \right)^{m_i} \hat{f} \left(\sum_{l=1}^N \Lambda_{l1} \hat{a}_l^\dagger \right) |0\rangle^{\otimes N}. \end{aligned} \quad (25)$$

We can see immediately from Eq. (25) that the effect of the beam splitter network is to mix the photonic creation operators of signal and auxiliary modes. At this point we use a well-known ordering formula

$$\left[\hat{a}, \hat{F}(\hat{a}, \hat{a}^\dagger) \right] = \frac{\partial}{\partial \hat{a}^\dagger} \hat{F}(\hat{a}, \hat{a}^\dagger) \quad (26)$$

to rewrite Eq. (25) in the convenient form

$$|\psi'\rangle \propto {}^{N-1}\langle 0 | \prod_{i,j=2}^N \frac{\left(\frac{\partial}{\partial \hat{a}_j^\dagger} \right)^{n_j}}{\sqrt{m_i! n_j!}} \left(\sum_{k=1}^N \Lambda_{ki} \hat{a}_k^\dagger \right)^{m_i} \hat{f} \left(\sum_{l=1}^N \Lambda_{l1} \hat{a}_l^\dagger \right) |0\rangle^{\otimes N}. \quad (27)$$

In the following we quote some basic results that follow immediately from Eq. (27). Suppose all $N - 1$ auxiliary modes are prepared in single-photon Fock states, and all $N - 1$ photodetectors find only the vacuum state at the respective output ports. Then the output is proportional to the $N - 1$ -fold application of the creation operator $(\hat{a}_1^\dagger)^{N-1}$. Similarly, if all auxiliary modes are prepared in the vacuum state and all photodetectors find exactly one

photon each, then the output is proportional to \hat{a}_1^{N-1} . These results should not be surprising if one remembers that we are merely selecting a particular measurement result from a passive linear operation which preserves photon numbers. Somewhat more interesting is the situation in which all auxiliary modes are occupied by single photons and all detectors register a photon each. Then the associated conditional operator is a polynomial of degree $N - 1$ in the number operator \hat{n}_1 , $P_{N-1}(\hat{n}_1)$. The last result is particularly important since it allows us to act upon the (unknown) coefficients of an N -dimensional signal mode *independently*.

3.3 Construction of simple quantum gates

”The permanent doesn’t really interact well with linear algebra.”
— Mark Jerrum, private communication

The theory outlined above presents the framework which we will use to construct particularly simple and useful quantum gates. For simplicity, we first restrict ourselves to single-mode gates and give an outlook to multi-mode gates later. We also assume that we want to operate within Fock layers, i.e. we merely change phases of some expansion coefficients. The simplest nontrivial operations can be generated with signal modes that contain up to two photons.⁶ Let us therefore consider the nonlinear phase shift gate \hat{C}_φ which is defined by its action on a three-dimensional single-mode state as

$$c_0|0\rangle + c_1|1\rangle + c_2|2\rangle \xrightarrow{\hat{C}_\varphi} c_0|0\rangle + c_1|1\rangle + e^{i\varphi}c_2|2\rangle. \quad (28)$$

According to what we have said earlier, in order to be able to act upon the coefficients of this three-dimensional signal state independently, we need a second-order polynomial in the number operator. Hence, we immediately find a network that performs the sought gate operation. The result is shown in Fig. 12. Note the triangular-shaped arrangement of the beam splitters as

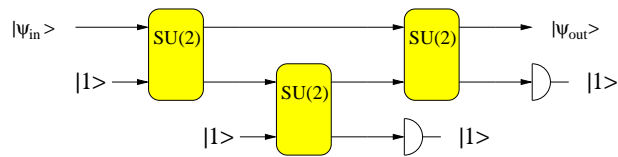


Fig. 12. $SU(3)$ network realizing the nonlinear phase shift.

predicted in [20].

⁶Note that all operations of the type $c_0|0\rangle + c_1|1\rangle \mapsto c_0|0\rangle + e^{i\varphi}c_1|1\rangle$ can be realized deterministically, since they are merely phase shifts.

Let us now analyze this network along the lines described above. We denote by \mathbf{A} the unitary (3×3) -matrix associated with the $SU(3)$ network. The conditional operator \hat{Y} acting on the signal mode is then

$$\begin{aligned} \hat{Y}_1|\psi\rangle &= c_0 \text{per } \mathbf{A}(1|1)|0\rangle + c_1 \text{per } \mathbf{A}|1\rangle \\ &+ c_2(2A_{11} \text{per } \mathbf{A} - A_{11}^2 \text{per } \mathbf{A}(1|1) + 2A_{12}A_{21}A_{13}A_{31})|2\rangle \end{aligned} \quad (29)$$

where $\text{per } \mathbf{A}$ denotes the permanent of the matrix \mathbf{A} and $\text{per } \mathbf{A}(1|1)$ its principal subpermanent. In order to realize a nonlinear phase shift, we need to fulfil the relations

$$\text{per } \mathbf{A}(1|1) = \text{per } \mathbf{A}, \quad \text{per } \mathbf{A}(1|1) [e^{i\varphi} + A_{11}^2 - 2A_{11}] = 2A_{12}A_{21}A_{13}A_{31}. \quad (30)$$

It turns out that there are infinitely many solutions to these equations which differ in their respective success probabilities. We have found numerically that the maximal probability is $1/4$ [22].

Permanents

The appearance of permanents in these problems is generic. The permanent of an $(n \times n)$ matrix \mathbf{A} is a generalized matrix function, defined as

$$\text{per } \mathbf{A} = \sum_{\{\sigma_i\} \in S_n} \prod_{i=1}^n A_{i\sigma_i} \quad (31)$$

where S_n is the group of cyclic permutations [23]. Permanents naturally appear in combinatorical problems, graph theory and related subjects. In our context they ‘count’ the ways of redistributing N single photons through an $SU(N)$ network to yield exactly N single photons at the outputs, i.e.

$$\text{per } \mathbf{A} = {}^{N \otimes} \langle 1 | \hat{U}_{12\dots N} | 1 \rangle^{\otimes N}. \quad (32)$$

As one can see from Eq. (29), the unitary network has to be adjusted such that the permanent and certain subpermanents of the associated unitary matrix fulfil certain relations. Furthermore, the overall success probability is just $|\text{per } \mathbf{A}(1|1)|^2$. Therefore, the optimal network is obtained by maximizing some permanent under a number of given constraints.

This is, in fact, a nontrivial task which is partly due to the fact that the algebraic property of a matrix being unitary does not imply any major simplifications for computing permanents.⁷ One of the few known fact is that permanents of unitary matrices are bounded from above. This is a consequence of the Marcus–Newman theorem [23] which states that for all $(m \times n)$ -matrices \mathbf{U} and $(n \times m)$ -matrices \mathbf{V} the inequality

⁷This is in stark contrast to the determinant which is just the product of the eigenvalues of a matrix.

$$|\text{per } \mathbf{UV}|^2 \leq \text{per } \mathbf{UU}^* \text{per } \mathbf{VV}^* \quad (33)$$

holds which reduces, when setting $\mathbf{V} = \mathbf{I}$ and regarding \mathbf{U} as being unitary, to $|\text{per } \mathbf{U}| \leq 1$. This is, of course, what one suspects if the permanent is supposed to be related to a success probability.

Another interesting fact to note is that computing permanents of matrices of increasingly larger size is a computationally hard problem in the sense that the computing time scales exponentially with the size of the matrix. Computer scientists say this problem is NP-complete. It seems that this computational problem is related to our quest to design quantum networks that would eventually be able to solve problems in polynomial rather than exponential time. That is, we have to solve an exponentially hard problem *first* by designing networks in order to avoid it *later* when applying them to unknown quantum states in the course of a quantum computation. Note however, that this argument strictly applies only if one is interested in the optimal network. For most practical purposes it is sufficient to approximate the permanent which can be done efficiently with a quadratic number of steps.

Dimension of the auxiliary state

What we have said so far about the nonlinear phase shift gate regarded the explicit construction of conditional nonlinear operators. It turns out, however, that this way of designing quantum gates, although being algorithmically transparent, does not yield optimal networks in terms of resources. For example, there is an alternative network proposed in Ref. [24] that also realizes the nonlinear phase shift but with one fewer beam splitter (see Fig. 13). As

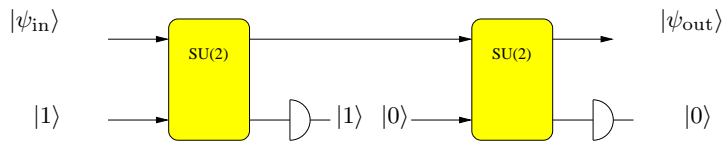


Fig. 13. Nonlinear sign shift gate with two beam splitters.

we will see later, the best networks for multi-dimensional quantum gates in terms of their respective success probabilities are not derived in this manner.

What seems to influence the required resources most is the dimensionality of the used auxiliary state. Comparing Fig. 12 and Fig. 13 one realizes that the Hilbert spaces spanned by the auxiliary modes are different in both cases. Starting from a product state of the form $|11\rangle$ as in Fig. 12, by beam splittings we actually span a three-dimensional space formed of the basis states $\{|20\rangle, |11\rangle, |02\rangle\}$. On the contrary, with an initial product state of the form $|10\rangle$ as in Fig. 13 we merely span a two-dimensional space with basis states

$\{|10\rangle, |01\rangle\}$. From this observation we can conclude that it is the dimensionality of the Hilbert space of the auxiliary modes that determines our ability to design quantum networks with the least possible resources.

3.4 Multi-mode gates

Similarly to the construction of single-mode quantum gates such as the nonlinear phase shift, we can proceed to more complex networks by referring to the results obtained before. The idea is rather simple. Let us restrict our attention again to quantum operations within a certain Fock layer, i.e. a subspace of the total Hilbert space of a multimode system with fixed photon number. Then we construct an M -mode quantum gate in the following way:

1. first feed the M modes into a generalized Mach–Zehnder interferometer with M input and output ports ($2M$ -port for short),
2. then act upon each output mode with an appropriate single-mode gate,
3. and finally recombine the M modes at another $2M$ -port.

Note that the first and last steps are done deterministically.

Consider for example the controlled-phase gate whose truth table is given in table 2. Because it represents a two-mode gate acting in the Fock layer with total photon number equal to two, this gate serves as the prime example for our statement. In terms of photonic amplitude operators, the conditional operator associated with the controlled-phase gate is given by

$$\hat{C}_\varphi = 1 - (1 - e^{i\varphi})\hat{n}_1\hat{n}_2, \quad (34)$$

where we have already written the operator in the simplest form that matches the dimensionality of the signal-mode Hilbert spaces.⁸ If we decompose the operator \hat{C}_φ into a product of two unitary operators associated with the Mach–Zehnder interferometer sandwiching some other nonlinear operator we find that these nonlinear operator indeed forms a tensor product $\hat{N}_1 \otimes \hat{N}_2$ of two single-mode conditional operators corresponding to nonlinear phase shift each of which has the form

$$\hat{N}_i = 1 - \frac{1}{2}(1 - e^{i\varphi})\hat{n}_i(\hat{n}_i - 1), \quad i = 1, 2. \quad (35)$$

Thus, combining all results we have obtained so far, we end up with a network depicted in Fig. 14. With the knowledge about the maximal success probability for a nonlinear sign flip (a nonlinear phase shift with $\varphi = \pi$) being $1/4$, the corresponding success probability of the controlled-phase gate will be $1/16$.

As we have already mentioned, this is not the highest probability one can actually achieve with linear optics and photodetection. The ‘record’ up

⁸Here we assume that the two-mode signal state is indeed only formed by the basis states $\{|00\rangle, |10\rangle, |01\rangle, |11\rangle\}$ without contributions from multi-photon states.

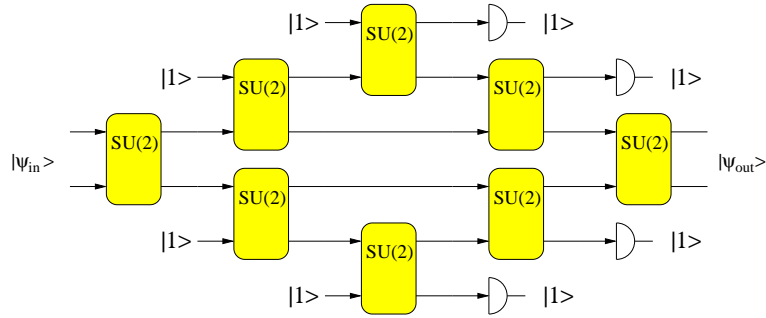


Fig. 14. Controlled-phase gate as two nonlinear phase shifts inside a balanced Mach-Zehnder interferometer.

until now is set by Ref. [25] where a network has been found that works with a probability of $2/27$. This network does not have the structure we have discussed here.

3.5 Conditional dynamics and scaling of success probabilities

In connection with the original proposal on using post-selection of subdynamics it has been suggested that the use of conditional dynamics could eventually yield success probabilities that are arbitrary close to unity. What is meant by conditional dynamics is that depending on a certain measurement outcome (or pattern for more detectors) the resulting output state is either retained (in case the measurement gave the wanted answer) or post-processed using the knowledge about the transformation due to the detection result. We will give a simple argument that within the framework of qubits being encoded in photon numbers this cannot hold.

For this purpose, let us return to the single-mode gate described earlier. Suppose therefore we had a single-mode quantum state of the form $c_0|0\rangle + c_1|1\rangle + c_2|2\rangle$ at hand and we send it through the arrangement of beam splitters as depicted in Fig. 13. After the first beam splitter which is fed with an auxiliary single photon the output can contain as much as three photons in one output port. Hence, there is a certain probability that two or three photons are found in the photodetector. Let us look at the extreme case in which all three photons end up in the detector. By conservation of photon numbers, the output state contains only vacuum. But that means that we have *lost all information* about the signal state which was originally encoded in the weights c_i of the superposition. If we detected two photons instead we would lose the information contained in c_0 . Thus, we can conclude that conditional dynamics breaks down if the total of number of photons measured in all photodetectors exceeds the total number of photons in the auxiliary state. Having said that, the obvious way of rescuing this situation is by noting that we have taken the measurements to be *projective* measurements. If in

future one finds a way of performing non-destructive (QND) measurements, one has immediately circumvented the information loss since all that has happened is a unitary transformation of the signal state.

Up until now, we have to live with projective measurements and it makes sense to ask what probabilities can be achieved in principle for certain gates and how they scale with increasing dimensionality of the signal state. We have already seen that the nonlinear sign flip can be realized with $p = 1/4$. In view of the algorithm to design multi-mode gates using generalized Mach–Zehnder interferometers, we could ask what the respective success probabilities are if we started from an $N + 1$ -dimensional signal state of the form $c_0|0\rangle + c_1|1\rangle + \dots + c_N|N\rangle$ and we would like to design a network that realizes a sign flip on the coefficient c_N . Then it turns out that if one used an N -dimensional auxiliary state with the lowest possible photon numbers, i.e. photon numbers in the range $0 \dots N - 1$, there are networks that achieve a the desired transformation with a probability of exactly $1/N^2$ [26].

4 Decoherence mechanisms — QED in causal dielectric media

”Please mind the gap between the hope and the reality.”

— Smoke #2

4.1 Decoherence mechanisms affecting atoms and photons

Trapping losses near current-carrying wires

As discussed in Sec. 2, the time the trapped atoms spend above the current-carrying wire is limited by several loss and heating mechanisms. In Ref. [13] one can find a table with several loss mechanisms relevant for atom chip experiments. We summarize the most important ones in table 3 and give their approximate associated lifetimes. Most of the loss mechanisms are in

Table 3. Loss mechanisms for trapped atoms above current-carrying wires

mechanism	lifetime
thermally induced spin flips	1 – 10s
technical noise	> 10s
background collisions	> 10s

fact avoidable as they are merely technical noise or account for experimental imperfections. Technical noise can cause both heating and spin flips. Heating processes are associated with low-frequency noise that causes the atoms in

the trap to be excited into higher vibrational modes. Spin flips, on the other hand, are induced by rf noise. Suppose an atom stayed 1s over the wire. The Rabi frequency that induces the spin flips is therefore 0.5Hz, which in turn is approximately given by 10^6Hz/G . Therefore, the rf magnetic field must be less than $1\mu\text{G}$ which, for an atom being 1mm away from the wire, amounts to current fluctuations of less than $1\mu\text{A}$. For a current of $1 - 10\text{A}$ needed to produce the dc magnetic field this means that the power supply must be unusually stable. This challenging but achievable.

However, some loss mechanisms are inherent in the way the atoms are trapped and can hardly be avoided. Most notable of these unavoidable losses is that caused by thermally induced spin flips which incidentally already gives rise to the biggest loss rate in current experiments [27]. In Figure 15 we show the five magnetic sublevels of the $|F=2\rangle$ -state of ^{87}Rb . In the experiment, the atoms are optically pumped into the $|F=2, m=2\rangle$ sublevel in which they are trapped. Spin flips induced by fluctuating magnetic fields cause the atom to jump into lower-lying magnetic sublevels in which they are either lost due to gravitational forces ($|F=2, m=0\rangle$) or expelled from the trap ($|F=2, m=-1\rangle$ and $|F=2, m=-2\rangle$). These spin-flip transitions are caused by magnetic-field fluctuations that are unavoidable as soon as metallic or dielectric materials are located close to the atoms. This is quite obviously the case in atom chips. In order to see where these fluctuations come from, we have to look deeper into the statistical implications of macroscopic (quantum) electrodynamics.

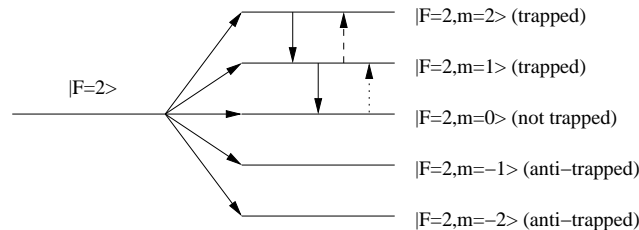


Fig. 15. Zeeman splitting of the $|F = 2\rangle$ state of ^{87}Rb and some of the possible spin-flip transitions.

Gate fidelity with imperfect linear optical elements

In Sec. 3 on all-optical realisations of quantum information processing with passive linear optical elements we have seen that the fidelity of a gate operation will depend crucially on the ability to generate single photons with very high efficiency and the amount of losses that are introduced by imperfect passive elements and photodetectors. It is not difficult to imagine that the purity of the ancilla photons used to operate a quantum circuit will have enormous influence on the way the quantum gates operates. For example,

an ancilla state consisting of a *mixture* of vacuum and a single-photon Fock state actually corresponds to realising *two different* quantum gates at once or, in other words, a statistical mixture of their respective operations. Another example of a decoherence process is provided by the inherent absorption in the passive linear optical elements used to build up the quantum circuit. An absorbing beam splitter does *not* act unitarily on the electromagnetic field modes impinging on it, but rather as a general CP map, i.e. as a statistical mixture of the desired and some unwanted operations.

All the loss and decoherence mechanisms sketched above can be described by a single and powerful theory which we will outline in this section.

4.2 Field quantisation in causal media

”Die ganzen Jahre bewußter Grübeleien haben mich der Antwort der Frage ‘Was sind Lichtquanten’ nicht näher gebracht. Heute glaubt zwar jeder Lump, er wisse es, aber er täuscht sich.”

— Albert Einstein, from a letter to Michele Besso (1951)

Quantum electrodynamics (or QED for short) is a well-established theory, and one might wonder how it is possible to obtain fundamentally new results apart from those that are already known. The answer comes about when considering *phenomenological* electrodynamics and when trying to quantize it.

Classical electrodynamics with media

Maxwell’s equations of the electromagnetic field in free space, i.e. without external sources, in temporal Fourier space can be cast in the following form:

$$\nabla \cdot \mathbf{B}(\mathbf{r}, \omega) = 0, \quad (36)$$

$$\nabla \cdot \mathbf{D}(\mathbf{r}, \omega) = 0, \quad (37)$$

$$\nabla \times \mathbf{E}(\mathbf{r}, \omega) = i\omega \mathbf{B}(\mathbf{r}, \omega), \quad (38)$$

$$\nabla \times \mathbf{H}(\mathbf{r}, \omega) = -i\omega \mathbf{D}(\mathbf{r}, \omega). \quad (39)$$

These equations have to be supplemented by appropriate constitutive relations which connect the electric field $\mathbf{E}(\mathbf{r}, \omega)$ and the magnetic induction $\mathbf{B}(\mathbf{r}, \omega)$ with the displacement field $\mathbf{D}(\mathbf{r}, \omega)$ and the magnetic field $\mathbf{H}(\mathbf{r}, \omega)$ which also carry information about the material. Assuming a purely dielectric medium, i.e. disregarding magnetic properties, one usually defines a polarisation field $\mathbf{P}(\mathbf{r}, \omega)$ via

$$\mathbf{D}(\mathbf{r}, \omega) = \varepsilon_0 \mathbf{E}(\mathbf{r}, \omega) + \mathbf{P}(\mathbf{r}, \omega). \quad (40)$$

In real space and assuming locally and linearly responding media, the polarisation can be written as a temporal convolution

$$\mathbf{P}(\mathbf{r}, t) = \varepsilon_0 \int_0^\infty d\tau \chi(\mathbf{r}, \tau) \mathbf{E}(\mathbf{r}, t - \tau) + \mathbf{P}_N(\mathbf{r}, t) \quad (41)$$

with the linear susceptibility $\chi(\mathbf{r}, \tau)$, the Fourier transform of which is related to the dielectric permittivity $\varepsilon(\mathbf{r}, \omega)$ by

$$\varepsilon(\mathbf{r}, \omega) = \chi(\mathbf{r}, \omega) + 1. \quad (42)$$

The permittivity is a complex function of frequency, $\varepsilon(\mathbf{r}, \omega) = \varepsilon_R(\mathbf{r}, \omega) + i\varepsilon_I(\mathbf{r}, \omega)$. The real and imaginary parts, which are responsible for dispersion and absorption, respectively, are related to each other by the Kramers–Kronig relations

$$\varepsilon_R(\mathbf{r}, \omega) - 1 = \frac{1}{\pi} \mathcal{P} \int d\omega' \frac{\varepsilon_I(\mathbf{r}, \omega')}{\omega' - \omega}, \quad (43)$$

$$\varepsilon_I(\mathbf{r}, \omega) = -\frac{1}{\pi} \mathcal{P} \int d\omega' \frac{\varepsilon_R(\mathbf{r}, \omega') - 1}{\omega' - \omega} \quad (44)$$

with \mathcal{P} denoting the principal value. The complex permittivity is an analytic function in the upper complex half-plane without zeros and satisfies the relation

$$\varepsilon(\mathbf{r}, -\omega^*) = \varepsilon^*(\mathbf{r}, \omega). \quad (45)$$

Furthermore, it approaches unity in the high-frequency limit. These analyticity properties, which carry over to the Green function to be defined later, will be important for proving equal-time commutation relations (ETCR for short) between electromagnetic field operators. This list of properties can be shown to follow from causality.

Equation (41) contains an additional, non-convolutive term $\mathbf{P}_N(\mathbf{r}, t)$. In fact, the existence of this term is crucial for the functioning of the following quantisation procedure. It serves as a Langevin noise source which is needed to preserve the ETCR. From statistical physics it is known that dissipation processes (as described by the imaginary part of the dielectric permittivity) are always accompanied by additional fluctuations. In order to see this more clearly, assume a damped harmonic oscillator with the solution for the expectation values $\langle \hat{a}(t) \rangle = \langle \hat{a}(t') \rangle e^{-\Gamma(t-t')}$. This relation cannot be valid in operator form since with increasing time the ETCR between $\hat{a}(t)$ and $\hat{a}^\dagger(t)$ would decay exponentially and eventually violates Heisenberg's uncertainty relations. Certainly, it is possible to add a Langevin force with vanishing expectation value to the oscillator which takes care of the ETCR. The noise polarisation $\mathbf{P}_N(\mathbf{r}, t)$ is exactly such a Langevin force. Its strength is determined by the linear fluctuation-dissipation theorem [28]. Assuming that $\mathbf{P}_N(\mathbf{r}, t)$ is proportional to a Gaussian random variable $\mathbf{f}(\mathbf{r}, \omega)$ which is always possible in linear reponse theory, and noting that the linear fluctuation-dissipation theorem states that the correlation function $\langle \mathbf{P}(\mathbf{r}, \omega), \mathbf{P}(\mathbf{r}', \omega') \rangle$ is proportional to

the imaginary part of the response function — hence the dielectric permittivity — we immediately deduce that the correct form of the noise polarisation must be [29, 30, 31]

$$\mathbf{P}_N(\mathbf{r}, t) = i\sqrt{\frac{\hbar\varepsilon_0}{\pi}}\varepsilon_I(\mathbf{r}, \omega)\mathbf{f}(\mathbf{r}, \omega). \quad (46)$$

As a matter of fact, the $\mathbf{f}(\mathbf{r}, \omega)$ plays the rôle of the fundamental variable in terms of which all relevant quantities can be expressed. Consider for example the Helmholtz equation for the electric field which is obtained by substituting Faraday's law (38) into Amperè's law (39) and using the constitutive relation (40) as

$$\nabla \times \nabla \times \mathbf{E}(\mathbf{r}, \omega) - \frac{\omega^2}{c^2}\varepsilon(\mathbf{r}, \omega)\mathbf{E}(\mathbf{r}, \omega) = \mu_0\omega^2\mathbf{P}_N(\mathbf{r}, \omega). \quad (47)$$

The solution to Eq. (47) is easily found to be

$$\mathbf{E}(\mathbf{r}, \omega) = \mu_0\omega^2 \int d^3\mathbf{s} \mathbf{G}(\mathbf{r}, \mathbf{s}, \omega) \cdot \mathbf{P}_N(\mathbf{s}, \omega) \quad (48)$$

where the (tensor-valued) Green function satisfies

$$\nabla \times \nabla \times \mathbf{G}(\mathbf{r}, \mathbf{s}, \omega) - \frac{\omega^2}{c^2}\varepsilon(\mathbf{r}, \omega)\mathbf{G}(\mathbf{r}, \mathbf{s}, \omega) = \delta(\mathbf{r} - \mathbf{s})\mathbf{U}, \quad (49)$$

where \mathbf{U} denotes the unit dyad. Equation (48) shows explicitly how all field quantities can eventually be expressed, via the noise polarisation, in terms of the fundamental field $\mathbf{f}(\mathbf{r}, \omega)$. As mentioned earlier, the dyadic Green function $\mathbf{G}(\mathbf{r}, \mathbf{s}, \omega)$, being a causal response function itself, has all the analytic properties the dielectric permittivity has, i.e. it is holomorphic in the upper complex frequency half-plane and satisfies the relation

$$\mathbf{G}(\mathbf{r}, \mathbf{s}, -\omega^*) = \mathbf{G}^*(\mathbf{r}, \mathbf{s}, \omega). \quad (50)$$

Moreover, it fulfils a generalized Onsager–Machlup reciprocity [28] relation of the form

$$\mathbf{G}(\mathbf{s}, \mathbf{r}, \omega) = \mathbf{G}^T(\mathbf{r}, \mathbf{s}, \omega). \quad (51)$$

From the partial differential equation (49) it also follows that the dyadic Green function satisfies an important integral relation,

$$\int d^3\mathbf{s} \frac{\omega^2}{c^2}\varepsilon_I(\mathbf{s}, \omega)\mathbf{G}(\mathbf{r}, \mathbf{s}, \omega) \cdot \mathbf{G}^+(\mathbf{r}', \mathbf{s}, \omega) = \text{Im}\mathbf{G}(\mathbf{r}, \mathbf{r}', \omega), \quad (52)$$

which expresses the fluctuation-dissipation theorem.

Quantized electrodynamics with media

The theory described above can now be quantized by regarding the fundamental field $\mathbf{f}(\mathbf{r}, \omega)$ as a bosonic vector field $\hat{\mathbf{f}}(\mathbf{r}, \omega)$ with the commutation rule

$$\left[\hat{\mathbf{f}}(\mathbf{r}, \omega), \hat{\mathbf{f}}^\dagger(\mathbf{r}', \omega') \right] = \delta(\mathbf{r} - \mathbf{r}') \delta(\omega - \omega') \mathbf{U}. \quad (53)$$

Then, for example the Fourier component of the electric field operator can be written, on using Eq. (48), as

$$\hat{\mathbf{E}}(\mathbf{r}, \omega) = i \sqrt{\frac{\hbar}{\pi \epsilon_0}} \frac{\omega^2}{c^2} \int d^3 \mathbf{s} \sqrt{\epsilon_I(\mathbf{s}, \omega)} \mathbf{G}(\mathbf{r}, \mathbf{s}, \omega) \cdot \hat{\mathbf{f}}(\mathbf{s}, \omega). \quad (54)$$

The corresponding Schrödinger operator is obtained by integrating over all frequency,

$$\hat{\mathbf{E}}(\mathbf{r}) = \int_0^\infty d\omega \hat{\mathbf{E}}(\mathbf{r}, \omega) + \text{h.c.} . \quad (55)$$

The so-defined operators fulfil all the requirements one imposes on a statistical quantum field theory. Firstly, the ETCR between electric field and magnetic induction can be shown to be [29, 30, 31]

$$\left[\hat{\mathbf{E}}(\mathbf{r}), \hat{\mathbf{B}}(\mathbf{r}') \right] = -\frac{i\hbar}{\epsilon_0} \nabla \times \delta(\mathbf{r} - \mathbf{r}') \mathbf{U}. \quad (56)$$

Secondly, the theory is — by construction — also consistent with the fluctuation-dissipation theorem which we can cast in the form

$$\langle 0 | \hat{\mathbf{E}}(\mathbf{r}, \omega) \hat{\mathbf{E}}^\dagger(\mathbf{r}', \omega') | 0 \rangle = \frac{\hbar \omega^2}{\pi \epsilon_0 c^2} \text{Im} \mathbf{G}(\mathbf{r}, \mathbf{r}', \omega) \delta(\omega - \omega'). \quad (57)$$

Equation (57) tells us that the (vacuum) fluctuations of the electric field are given by the imaginary part of the Green function as one would expect. Finally, the Hamiltonian describing the electromagnetic field in the presence of absorbing matter is given by

$$\hat{H} = \int d^3 \mathbf{r} \int_0^\infty d\omega \hbar \omega \hat{\mathbf{f}}^\dagger(\mathbf{r}, \omega) \cdot \hat{\mathbf{f}}(\mathbf{r}, \omega) \quad (58)$$

which is diagonal in the fundamental bosonic vector field $\hat{\mathbf{f}}(\mathbf{r}, \omega)$. Maxwell's equations then follow from the Heisenberg equations of motion of the above-defined electromagnetic field operators.

Extensions of this theory to spatially anisotropic materials (for which the dielectric permittivity is a symmetric tensor) and media with gain can be found in [30, 31]. Magnetic materials, including the important class of magnetodielectrics or left-handed media, can be treated in a completely analogous way [32]. We will, however, not elaborate more on this subject as it is not needed for our present purposes.

4.3 Thermally induced spin flips near metallic wires

The above-described theory is now perfectly suitable to describe magnetic-field fluctuations radiated by metallic structures which cause spin flips between trapped and anti-trapped (or non-trapped) magnetic sublevels of atomic hyperfine ground states. The experiment in [27] used a coated wire to trap ^{87}Rb atoms in their $|F = 2, m = 2\rangle$ magnetic sublevel. The atoms are located at a distance r from the surface of the wire with radius a_2 (see Fig. 16).

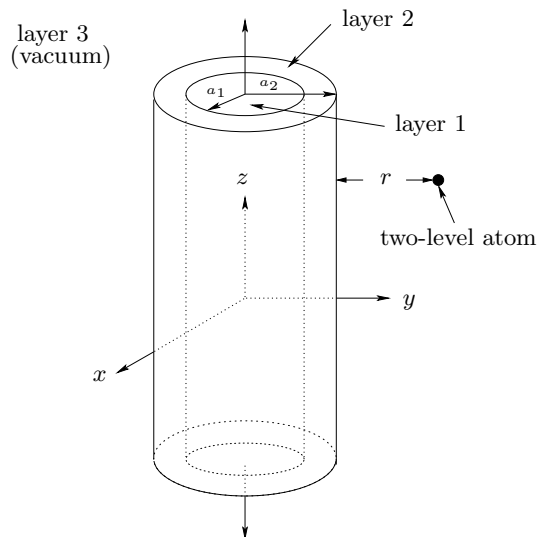


Fig. 16. A two-level atom is located at a distance r from the surface of a coated wire that runs along the z -direction.

The interaction of a neutral atom positioned at some point \mathbf{r}_A with the electromagnetic field described by the Hamiltonian (58) via the Zeeman interaction $\hat{H}_Z = -\hat{\boldsymbol{\mu}} \cdot \hat{\mathbf{B}}(\mathbf{r}_A)$ of the atom's magnetic moment $\hat{\boldsymbol{\mu}}$ with the magnetic field causes the spin of the atoms to flip. Since the atoms are in their respective (electronic) ground state, it is safe to assume that the angular momentum is zero. Moreover, the nuclear magnetic moment is small compared to the Bohr magneton μ_B . This leaves us with an expression for the atom's magnetic moment associated with the transition $|i\rangle \rightarrow |f\rangle$ as $\hat{\boldsymbol{\mu}} = \boldsymbol{\mu}|i\rangle\langle f| + \text{h.c.}$ where the magnitude $\boldsymbol{\mu}$ is given by the (electronic) spin matrix element $\boldsymbol{\mu} = 2\mu_B\langle i|\hat{\mathbf{S}}|f\rangle$. If we define the spin flip operators $\hat{\sigma} = |f\rangle\langle i|$ satisfying the angular-momentum algebra $[\hat{\sigma}, \hat{\sigma}_z] = \hat{\sigma}$, we can write the total Hamiltonian in rotating-wave approximation as

$$\hat{H} = \int d^3\mathbf{r} \int_0^\infty d\omega \hbar\omega \hat{\mathbf{f}}^\dagger(\mathbf{r}, \omega) \cdot \hat{\mathbf{f}}(\mathbf{r}, \omega) + \frac{1}{2}\hbar\omega_{fi}\hat{\sigma}_z - \left[\hat{\sigma}^\dagger \boldsymbol{\mu} \cdot \nabla \times \int_0^\infty d\omega \int d^3\mathbf{r} \frac{\omega}{c^2} \sqrt{\frac{\hbar}{\pi\epsilon_0}} \epsilon_I(\mathbf{r}, \omega) \mathbf{G}(\mathbf{r}_A, \mathbf{r}, \omega) \cdot \hat{\mathbf{f}}(\mathbf{r}, \omega) + \text{h.c.} \right]. \quad (59)$$

Using the Hamiltonian (59) in the Heisenberg equations of motion for the spin flip operators, we find after some calculation that in the Markov approximation the spin flip rate is given by [33]

$$\Gamma = \frac{8\mu_B^2}{\hbar\epsilon_0 c^2} \langle f | \hat{\mathbf{S}} | i \rangle \cdot \text{Im} [\nabla \times \nabla \times \mathbf{G}(\mathbf{r}_A, \mathbf{r}_A, \omega_{fi})] \cdot \langle i | \hat{\mathbf{S}} | f \rangle. \quad (60)$$

Taking into account that the flip rate is thermally enhanced, i.e. not only spontaneous but also stimulated (induced) flips occur, the rate (60) has to be modified by a multiplicative factor $(e^{\hbar\omega_{fi}/kT} - 1)^{-1}$ which is proportional to T for high temperature. Furthermore, considering the initial state $|i\rangle$ to be the $|F=2, m=2\rangle$ magnetic sublevel and the final state $|f\rangle$ to be the state $|F=2, m=1\rangle$, an additional factor of $1/4$ due to the expansion of the $|F, m\rangle$ -states in terms of the eigenstates of electronic and nuclear spin operators is present.

Now we are in a position to compare with experimental measurements. The experiment in [27] used a coated wire with a copper core of $185\mu\text{m}$ radius and an aluminium coating with $55\mu\text{m}$ thickness. The transition frequency between two neighboring magnetic sublevels was $f = \omega_{fi}/2\pi = 560\text{kHz}$. The result of the calculations with our theory and the experimental data are shown in Fig. 17 where we have plotted the inverse spin flip rate, hence the average lifetime τ of an atom in the trap. It is clear that our theoretical result will only serve as an upper bound on the lifetime since, as we have mentioned earlier, there are indeed other noise sources that influence the duration of stay of the atoms in their trap. Note, however, that the agreement is still astonishingly good which means that our earlier claim that most other noise source are negligible in this experiment, was indeed valid.

4.4 Imperfect passive optical elements

Another, seemingly unrelated, application of the field quantization in absorbing materials is found if we consider passive optical elements such as beam splitters under realistic conditions, i.e. including losses in the beam splitter material. As noted earlier, a lossless beam splitter acts upon the amplitude operators of the incoming waves as an $\text{SU}(2)$ group element [18]. That is, two amplitude operators $\hat{a}_1(\omega)$ and $\hat{a}_2(\omega)$ are transformed into new amplitude operators $\hat{b}_1(\omega)$ and $\hat{b}_2(\omega)$ as

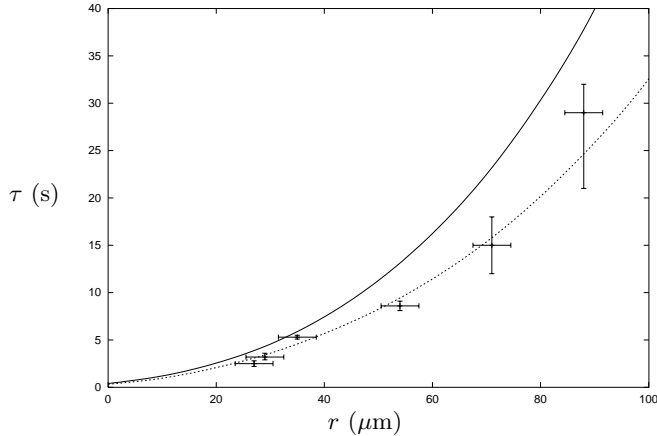


Fig. 17. Lifetime τ of the trapped atom as a function of the distance r from the surface of the current-carrying wire. The solid line corresponds to the calculated lifetime according to the theory presented in the text. The crosses represent experimental data points. The dotted line is the result for a slab-geometry according to [34].

$$\begin{pmatrix} \hat{b}_1(\omega) \\ \hat{b}_2(\omega) \end{pmatrix} = \mathbf{T}(\omega) \begin{pmatrix} \hat{a}_1(\omega) \\ \hat{a}_2(\omega) \end{pmatrix} \quad (61)$$

where $\mathbf{T}(\omega)$ is a unitary matrix, i.e. $\mathbf{T}(\omega)\mathbf{T}^+(\omega) = \mathbf{I}$. For lossy beam splitters, this is certainly not true since some of the electromagnetic radiation impinging on the beam splitter will actually be absorbed. This process can be accounted for by introducing an absorption matrix $\mathbf{A}(\omega)$ in order to satisfy the energy conservation $\mathbf{T}(\omega)\mathbf{T}^+(\omega) + \mathbf{A}(\omega)\mathbf{A}^+(\omega) = \mathbf{I}$. Both matrices actually follow from a decomposition of the associated Green function into contributions associated with travelling waves moving to the left and right [35] and are therefore given by the complex refractive-index profile of the beam splitter material and geometric parameters.

However, it turns out that, associating the material excitations with some bosonic variables $\hat{g}_1(\omega)$ and $\hat{g}_2(\omega)$ which are special linear combinations of the fundamental bosonic field variables $\hat{\mathbf{f}}(\mathbf{r}, \omega)$ restricted to one spatial dimension [35], the beam splitter acts unitarily on the combined set of photonic and material amplitude operators [36]. In fact, a lossy beam splitter can be represented as an $\text{SU}(4)$ group element. That is, the ‘four-vector’ $\hat{\alpha}(\omega)$ consisting of incoming photonic amplitude operators and the material excitations transforms unitarily into the ‘four-vector’ $\hat{\beta}(\omega)$ of outgoing photonic amplitude operators and some new matter operators, i.e.

$$\hat{\beta}(\omega) = \mathbf{A}(\omega)\hat{\alpha}(\omega), \quad \mathbf{A}(\omega)\mathbf{A}^+(\omega) = \mathbf{I}. \quad (62)$$

The unitary 4×4 -matrix $\mathbf{A}(\omega)$ can be decomposed into block form as

$$\mathbf{A}(\omega) = \begin{pmatrix} \mathbf{T}(\omega) & \mathbf{A}(\omega) \\ -\mathbf{S}(\omega)\mathbf{C}^{-1}(\omega)\mathbf{T}(\omega) & \mathbf{C}(\omega)\mathbf{S}^{-1}(\omega)\mathbf{T}(\omega) \end{pmatrix} \quad (63)$$

where $\mathbf{C}(\omega) = \sqrt{\mathbf{T}(\omega)\mathbf{T}^+(\omega)}$ and $\mathbf{S}(\omega) = \sqrt{\mathbf{A}(\omega)\mathbf{A}^+(\omega)}$ are commuting positive Hermitian 2×2 -matrices. The associated unitary operator \hat{U} that realizes the transformation $\hat{\beta}(\omega) = \mathbf{A}(\omega)\hat{\alpha}(\omega) = \hat{U}^\dagger \hat{\alpha}(\omega) \hat{U}$ is then obtained as

$$\hat{U} = \exp \left\{ -i \int_0^\infty d\omega [\hat{\alpha}^\dagger(\omega)]^T \boldsymbol{\Phi}(\omega) \hat{\alpha}(\omega) \right\} \quad (64)$$

where the matrix $\boldsymbol{\Phi}(\omega)$ is defined by $e^{-i\boldsymbol{\Phi}(\omega)} = \mathbf{A}(\omega)$. The operator \hat{U} and the matrix $\mathbf{A}(\omega)$ can be used as well to transform quantum states. For this purpose, let us assume that the density operator of the quantum state before the transformation is an operator functional of $\hat{\alpha}(\omega)$, i.e. $\hat{\rho} = \hat{\rho}[\hat{\alpha}(\omega), \hat{\alpha}^\dagger(\omega)]$. Then, transformation of the quantum state and tracing over the degrees of freedom associated with the beam splitter leaves us with

$$\hat{\rho}' = \text{Tr} \left\{ \hat{\rho} \left[\hat{U} \hat{\alpha}(\omega) \hat{U}^\dagger, \hat{U} \hat{\alpha}^\dagger(\omega) \hat{U}^\dagger \right] \right\}. \quad (65)$$

In quantum information theory, decoherence processes are frequently described by the Kraus decomposition of the quantum-state transformation (65). That is, we seek an operator decomposition of the form

$$\hat{\rho}' = \sum_i \hat{W}_i \hat{\rho} \hat{W}_i^\dagger, \quad \sum_i \hat{W}_i^\dagger \hat{W}_i = \hat{I}. \quad (66)$$

For this purpose, let us assume that the beam splitter is in its ground state, thereby neglecting thermal excitations which at room temperature and optical frequencies is a safe assumption. Let us also restrict ourselves to quasi-monochromatic radiation in which case we can drop all frequency dependencies. Then, calculating the partial trace in Eq. (65) in the coherent-state basis as

$$\hat{\rho}' = \frac{1}{\pi^2} \int d^2\alpha_3 d^2\alpha_4 \hat{W}_{\alpha_3, \alpha_4} \hat{\rho} \hat{W}_{\alpha_3, \alpha_4}^\dagger \quad (67)$$

where the continuous-index Kraus operators are defined by

$$\hat{W}_{\alpha_3, \alpha_4} = \langle \alpha_3, \alpha_4 | \hat{U} | 0_3, 0_4 \rangle, \quad (68)$$

we eventually find that the Kraus operators of an absorbing beam splitter are $(\exp -i\boldsymbol{\Phi}_T = \mathbf{T})$ [22]

$$\hat{W}_{\alpha_3, \alpha_4} = \exp \left(-i[\hat{\mathbf{a}}^\dagger]^T \boldsymbol{\Phi}_T \hat{\mathbf{a}} \right) \exp \left(-\boldsymbol{\alpha}^+ \mathbf{S} \mathbf{C}^{-1} \mathbf{T} \hat{\mathbf{a}} \right) \exp \left(-\boldsymbol{\alpha}^+ \boldsymbol{\alpha} / 2 \right). \quad (69)$$

One checks easily that these operators become unitary operators in the limit of vanishing absorption, i.e. when \mathbf{T} is unitary and therefore $\boldsymbol{\Phi}_T$ Hermitian, and \mathbf{S} vanishes. We also see that the term $\exp(-\boldsymbol{\alpha}^+ \mathbf{S} \mathbf{C}^{-1} \mathbf{T} \hat{\mathbf{a}})$ is responsible for absorption as it is a function of the annihilation operators only.

Other error sources

Apart from absorption in the dielectric material, there are several other sources of errors in an experimental implementation. So far, we have assumed that the auxiliary states are perfectly pure states, especially we have implicitly assumed that we are able to produce single photons on demand with very high efficiency. This, however, is an oversimplification. All realistic sources produce as most a mixed state of the form $(1-p)|0\rangle\langle 0| + p|1\rangle\langle 1|$ with efficiency p . The best single-photon sources to date achieve a single-photon efficiency of at most 80%. This means that the first beam splitter in Fig. 13 does not always act as a first-order polynomial in \hat{n} , but sometimes subtracts a photon from the signal state.

Another crucial error source are the detectors themselves. In our mathematical description we have assumed that the photodetectors are perfect and can therefore be described by a projection operator $|n\rangle\langle n|$. However, since they show losses themselves, we have to replace it by

$$|n\rangle\langle n| \mapsto \hat{\Pi}(n) = \sum_{k=n}^{\infty} \binom{k}{n} \eta^n (1-\eta)^{k-n} |k\rangle\langle k| \quad (70)$$

which constitutes a positive operator-valued measure (a generalization of a projective measurement). It describes the effect of absorption in the photodetector itself. The number η is commonly called the detector efficiency. Typical values for avalanche photo diodes are $\eta \approx 0.3$.

We can measure the effect of these error sources by introducing the gate fidelity F as the overlap between the wanted result $|\psi'\rangle$ and the achieved density matrix $\hat{\rho}$, i.e. $F = \langle \psi' | \hat{\rho} | \psi' \rangle$. Since the so-defined fidelity still depends on the chosen signal state — because not all signal states are effected in the same manner by the errors — we define an average fidelity \bar{F} by averaging over all possible signal states.

Figure 18 shows the effect of non-unit single-photon efficiency p (left figure) and detector efficiency η (right figure) on the average gate fidelity. One can see that even a small inefficiency in either the detection process or the preparation process of the auxiliary state results in a (roughly linear) drop in the gate fidelity. In a different setting, in which the quantum information is encoded in the superposition states of one photonic excitation in two modes, a similar behaviour has been observed [37]. This result has important consequences for the scalability of such gates since quantum error correction only works if the individual errors in the network components does not exceed $\approx 10^{-3}$ (see for example [38] and references cited therein). In other words, in order to be able to correct for errors, both discussed inefficiencies can be at most of the same order as the desired error rate which currently seems to be experimentally impossible.

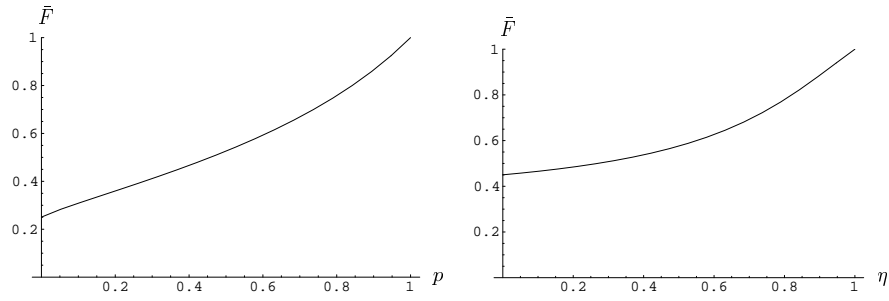


Fig. 18. Average gate fidelity with imperfect auxiliary photons (left figure) and imperfect detectors (right figure).

Acknowledgements

We would like to thank Dominic Berry, Matthew Jones, Norbert Lütkenhaus, Bill Munro, Kae Nemoto, Per-Kristian Rekdal and Barry Sanders for discussions and their input to the research reviewed here. This work was funded in parts by the UK Engineering and Physical Sciences Research Council (EPSRC), the Royal Society, and the European Commission (QUEST, QGATES, and FASTNET networks). Special thanks goes to John, publican of the Gowlett Arms, for providing one us with the necessary amount of Brains.

References

1. H. Rabitz, R. de Vivie-Riedle, M. Motzkus, and K. Kompa: *Science* **288**, 824 (2000); C.H. Bennett, J.I. Cirac, M.S. Leifer, D.W. Leung, N. Linden, S. Popescu, and G. Vidal: *Phys. Rev. A* **66**, 012305 (2002)
2. V. Bužek, M. Hillery, and R.F. Werner: *Phys. Rev. A* **60**, R2626 (1999)
3. D.P. DiVincenzo: *Phys. Rev. A* **51**, 1015 (1995)
4. D. Jaksch, C. Bruder, J.I. Cirac, C.W. Gardiner, and P. Zoller: *Phys. Rev. Lett.* **81**, 3108 (1998)
5. M. Greiner, I. Bloch, O. Mandel, T.W. Hänsch, and T. Esslinger: *Phys. Rev. Lett.* **87**, 160405 (2001); M. Greiner, O. Mandel, T. Esslinger, T.W. Hänsch, and I. Bloch: *Nature (London)* **415**, 39 (2002)
6. C. Orzel, A.K. Tuchman, M.L. Fenselau, M. Yasuda, and M.A. Kasevich: *Science* **291**, 2386 (2001)
7. D.S. Petrov, G.V. Shlyapnikov, and J.T.M. Walraven: *Phys. Rev. Lett.* **85**, 3745 (2000)
8. V. Dunjko, V. Lorent, and M. Olshanii: *Phys. Rev. Lett.* **86**, 5413 (2001)
9. M.P.A. Fisher, P.B. Weichman, G. Grinstein, and D.S. Fisher: *Phys. Rev. B* **40**, 546 (1989)
10. J. Pachos and P.L. Knight: *Phys. Rev. Lett.* **91**, 107902 (2003)
11. O. Mandel, M. Greiner, A. Widera, T. Rom, T.W. Hänsch, and I. Bloch: *Phys. Rev. Lett.* **91**, 010407 (2003)

12. E.A. Hinds and I.A. Hughes: J. Phys. D: Appl. Phys. **32**, R119 (1999)
13. R. Folman, P. Krüger, J. Schmiedmayer, J. Denschlag, and C. Henkel: Adv. At. Mol. Opt. Phys. **48**, 263 (2002)
14. E.A. Hinds: Phil. Trans. R. Soc. Lond. A **357**, 1409 (1999)
15. M. Koashi, T. Yamamoto, and N. Imoto: Phys. Rev. A **63**, 030301 (2001)
16. T.B. Pittman, B.C. Jacobs, and J.D. Franson: Phys. Rev. A **64**, 062311 (2001); T.B. Pittman, B.C. Jacobs, and J.D. Franson: Phys. Rev. Lett. **88**, 257902 (2002)
17. E. Knill, R. Laflamme, and G.J. Milburn: Nature (London) **409**, 46 (2001)
18. B. Yurke, S.L. McCall, and J.R. Klauder: Phys. Rev. A **33**, 4033 (1986); S. Prasad, M.O. Scully, and W. Martienssen: Opt. Commun. **62**, 139 (1987); Z.Y. Ou, C.K. Hong, and L. Mandel: Opt. Commun. **63**, 118 (1987); H. Fearn and R. Loudon, Opt. Commun. **64**, 485 (1987); M.A. Campos, B.E.A. Saleh, and M.C. Teich: Phys. Rev. A **40**, 1371 (1989); U. Leonhardt: Phys. Rev. A **48**, 3265 (1993)
19. K. Wodkiewicz and J.H. Eberly: J. Opt. Soc. Am. B **2**, 458 (1985)
20. M. Reck, A. Zeilinger, H.J. Bernstein, and P. Bertani: Phys. Rev. Lett. **73**, 58 (1994)
21. M. Byrd: Preprint arXiv:physics/9708015; T. Tilma, M. Byrd, and E.C.G. Sudarshan: J. Phys. A: Math. Gen. **35**, 10445 (2002)
22. S. Scheel, K. Nemoto, W.J. Munro, and Peter L. Knight: Phys. Rev. A **68**, 032310 (2003)
23. H. Minc: *Permanents* (Addison-Wesley, London, 1978)
24. T.C. Ralph, A.G. White, W.J. Munro, and G.J. Milburn: Phys. Rev. A **65**, 012314 (2001)
25. E. Knill: Phys. Rev. A **66**, 052306 (2002)
26. S. Scheel and N. Lütkenhaus: in preparation
27. M.P.A. Jones, C.J. Vale, D. Sahagun, B.V. Hall, and E.A. Hinds: Phys. Rev. Lett. **91**, 080401 (2003)
28. R.L. Stratonovich: *Nonlinear nonequilibrium thermodynamics I: linear and nonlinear fluctuation-dissipation theorems* (Springer, Heidelberg, 1992)
29. T.D. Ho, L. Knöll, and D.-G. Welsch: Phys. Rev. A **57**, 3931 (1998)
30. S. Scheel, L. Knöll, and D.-G. Welsch: Phys. Rev. A **58**, 700 (1998)
31. L. Knöll, S. Scheel, and D.-G. Welsch: QED in dispersing and absorbing dielectric media. In: *Coherence and Statistics of Photons and Atoms*, ed by J. Peřina (Wiley, New York, 2001) pp 1–64
32. T.D. Ho, S.Y. Buhmann, L. Knöll, D.G. Welsch, S. Scheel, and J. Kästel: Phys. Rev. A **68**, 043816 (2003)
33. P.K. Rekdal, S. Scheel, E.A. Hinds, and Peter L. Knight: in preparation
34. C. Henkel and, S. Pötting, and M. Wilkens: Appl. Phys. B **69**, 379 (1999)
35. T. Gruner and D.G. Welsch: Phys. Rev. A **54**, 1661 (1996)
36. L. Knöll, S. Scheel, E. Schmidt, D.G. Welsch, and A.V. Chizhov: Phys. Rev. A **59**, 4716 (1999)
37. G.J. Milburn, T.C. Ralph, A. Gilchrist, A.G. White, W.J. Munro, and V. Kendon: in Proceedings of the 6th International Conference on Quantum Communication, Measurement and Computing, Boston, July 2002, eds. J. Shapiro and O. Hirota (Rinton Press, Princeton, 2002)
38. A.M. Steane: Phys. Rev. A **68**, 042322 (2003)